Journal of Non-Newtonian Fluid Mechanics 166 (2011) 1221–1228

Contents lists available at ScienceDirect

Journal of Non-Newtonian Fluid Mechanics

journal homepage: http://www.elsevier.com/locate/jnnfm

An analysis of the effect of stress diffusion on the dynamics of creeping viscoelastic flow

Becca Thomases *

Department of Mathematics, University of California, Davis, CA 95616, United States

ARTICLE INFO

Article history:
Received 28 May 2011
Received in revised form 22 July 2011
Accepted 26 July 2011
Available online 6 August 2011

Keywords:
Viscoelastic fluid models
Stress diffusion
Oldroyd-B
FENE-P

ABSTRACT

The effect of stress diffusivity is examined in both the Oldroyd-B and FENE-P models of a viscoelastic fluid in the low Reynolds (Stokes) limit for a 2D periodic time-dependent flow. A local analytic solution can be obtained when assuming a flow of the form $\mathbf{u} = Wi^{-1}(x, -y)$, where Wi is the Weissenberg number. In this case the width of the birefringent strand of the polymer stress scales with the added viscosity as $\nu^{1/2}$, and is independent of the Weissenberg number. Also, the "expected" maximum extension of the polymer coils remains finite with any stress diffusion and scales as $Wi \cdot \nu^{-1/2}$. These predictions closely match the full simulations. As many investigations of viscoelastic fluids incorporate both finite extension as well as polymer stress diffusion we also investigate the FENE-P model with diffusion to see which effect dominates for various model parameters. With this penalization the percent of maximum extension can be predicted based on Wi, ν, and b, the maximum extensibility length.

1. Introduction

The inclusion of stress diffusivity is an important consideration in viscoelastic flow simulations. Large scale simulations, for example to understand turbulent drag reduction, require the use of stress diffusion for convergent calculations [1–8]. Even in investigations of micro-fluidic flows, say to study elastic turbulence [9–11], some stress diffusion is added to limit gradient growth in long-time simulations [12,13].

The potential for loss of smoothness of the stress tensor in the Oldroyd-B model has been known for some time [14,15] and it has been exhibited that these non-physical solutions arise in the long-time limit in both a local analytic model and in simulations of a simple four-roll mill background forcing [16]. A typical response to these numerical difficulties is to add diffusion to the advection equation of the polymer stress. This is not without physical justification as stress diffusion does arise in the physical model [17,18]. When derived from the kinetic theory of dumbbells the stress diffusion coefficient is proportional to the square of the ratio of the bead diameter (or polymer radius of gyration) to the flow length-scale and even in the context of micro-fluidics it is minute (10^{-6} at most). Hence artificially large polymer stress diffusion is introduced as a regularization parameter in numerical simulations. The effect of artificially large stress diffusion was studied in [19] where the authors concluded that the stress diffusion had a stabilizing effect, in particular for large Reynolds number calculations. The authors observe further that the diffusion did not have an appreciable effect on the flow. In this article we make these conclusions more precise in a special case. In particular we observe in our simulations and with a local model that the inclusion of any amount of polymer diffusion ($\nu > 0$) will yield a resultant stress that is smooth and bounded.

The special case studied here is inspired by [16]. In that paper, extensional points in the flow are created by fixing a steady background forcing which produces a four-roll mill geometry in a purely Newtonian Stokes flow. These extensional points are maintained when the polymer stress evolves from isotropic initial data. At these extensional points the authors find the emergence, exponentially in time, of singular structures in the polymer stress which closely match exact solutions they find for a local analytic model. The regularity of the singular structures decreases as the Weissenberg number increases. The velocity field rapidly approaches a steady-state that remains locally, about the central extensional point, a simple straining flow. The modification in this paper is the addition of polymer stress diffusion. With this we are still able to construct a local model which agrees well with the simulations and which has a closed form solution. This enables us to make some quantitative predictions about the effect of stress diffusion on the flow.

1.1. Equations of motion

We study numerically the two-dimensional equations of viscoelastic flow in the zero-Reynolds number limit. Biperiodic boundary conditions are assumed and persistent curvilinear flows are

* Tel.: +1 530 554 2988; fax: +1 530 752 6635.
E-mail address: thomases@math.ucdavis.edu

0377-0257/$ - see front matter © 2011 Elsevier B.V. All rights reserved.
doi:10.1016/j.jnnfm.2011.07.009

created by imposing a very simple body force. The system of equations governing the flow of a general viscoelastic fluid (in the zero-Reynolds number limit) can be written in dimensionless form as

$$-\nabla p + \Delta \mathbf{u} + \beta \nabla \cdot \mathbf{T} = \mathbf{f}, \quad \nabla \cdot \mathbf{u} = 0, \tag{1}$$

where $\beta = G\tau_f/\mu$ measures the relative contribution of the polymer stress to momentum balance. Here G is the isotropic stress in the polymer field in the absence of flow and $\tau_f = \mu/\rho L\, F$ the flow time scale, set by F the dimensional scale of the forcing, μ the solvent viscosity, ρ the fluid density, and L the system size. In Eq. (1), $\mathbf{T}$ represents the viscoelastic contribution to the extra stress. For an Oldroyd-B fluid, the extra stress tensor $\mathbf{T}$ is given in terms of the conformation tensor $\mathbf{S}$ as

$$\mathbf{T} = (\mathbf{S} - \mathbf{I}), \tag{2}$$

and for a FENE-P fluid, the extra stress tensor $\mathbf{T}$ is

$$\mathbf{T} = \left(\frac{\mathbf{S}}{1 - \frac{\mathrm{tr}\mathbf{S}}{b}} - \mathbf{I} \right). \tag{3}$$

The parameter b is proportional to the maximum polymer length. The evolution equation for the conformation tensor with diffusion is given by

$$Wi\left[\frac{\partial \mathbf{S}}{\partial t} + \mathbf{u} \cdot \nabla \mathbf{S} - \left(\nabla \mathbf{u}\mathbf{S} + \mathbf{S}\nabla \mathbf{u}^T\right)\right] = -\mathbf{T} + \nu \Delta \mathbf{S}, \tag{4}$$

here $Wi = \tau_p/\tau_f$ is the Weissenberg number, with τ_p the polymer relaxation time. The quantity $\beta \cdot Wi$ is the ratio of polymer to solvent viscosity so that given a particular working fluid, its value is fixed independent of experimental conditions. In the work of Arratia et al., [20] the value $\beta \cdot Wi \approx 0.5$ which is used in the majority of our simulations. We will make some comments regarding other values of $\beta \cdot Wi$ at the end of Section 2. The independent parameter ν is the polymer stress diffusion coefficient, as arises when including the effect of center of mass diffusion of polymer coils. The dimensionless stress diffusivity is defined as $\nu/Wi = D_s/(UL)$ where D_s is the stress diffusion coefficient.

The scale of the force $\mathbf{f}$ is used to set the flow time-scale, the time-scale of transport to be order one. The background force is given by

$$\mathbf{f} = \begin{pmatrix} -2\sin x \cos y \\ 2\cos x \sin y \end{pmatrix}. \tag{5}$$

In a purely Newtonian Stokes flow this forcing yields a four vortex "mixer" in each $[-\pi, \pi]^2$ cell.

The trace of $\mathbf{S}$ is an important physical quantity representing the amount of stretching of polymer coils. In [21] it was shown that global solutions to a FENE-P model with polymer diffusion exist as long as tr $\mathbf{S}$ is bounded and $\mathbf{S}$ is sufficiently smooth. Subsequent blow-up criteria (similar to the Beale–Kato–Majda criteria for the Euler equations [22]) for the Oldroyd-B model have been derived and show that as long as the L^∞ norm of the extra stress is integrable in time solutions will exist [23,24].

The numerical simulations for this work employ the square-root method for evolving the symmetric square root of the conformation tensor introduced in [25]. In that work an evolution equation which is equivalent to Eq. (4) is derived for $\mathbf{b}$ such that $\mathbf{b}$ is symmetric and $\mathbf{b}^T\mathbf{b} = \mathbf{S}$. In [25] improved accuracy and stability was shown for a pseudo-spectral application of the square-root method. One advantage of the square-root method is that the conformation tensor will be inherently symmetric positive definite. We find that for sufficiently large Wi or sufficiently small ν the square-root method is preferred and adds no major cost.

Our simulations are done with a pseudo-spectral method [26]. The square-root of the conformation tensor is evolved using a second-order Adams-Bashforth Crank-Nicholson method. The initial data (symmetric positive definite) for $\mathbf{b}$ is prescribed, and given $\mathbf{S} = \mathbf{b}^T\mathbf{b}$, the Stokes equation, Eq. (1), is inverted in Fourier space for $\mathbf{u}$. Given $\mathbf{u}$, the nonlinearities of the polymer stress evolution, Eq. (4), are evaluated and a smooth filter is applied in Fourier space before the quadratic terms are multiplied in real space; see [27] for details. The solutions are well resolved (due to the smoothness of the solutions and the choice of a spectral method) and spatial resolutions of $N^2 = 256^2$ are used in the simulations. In the following simulations initial data is isotropic $\mathbf{b}(0) = \mathbf{I}$. The flow relaxes to steady state after several multiples of Wi, and here all steady-state simulations are shown at $t = 10 \cdot Wi$.

2. Extensional flow

In [16] it was observed that for isotropic initial data $\mathbf{S}(0) = \mathbf{I}$, the velocity field approached a steady-state, *locally* near the extensional stagnation point at the origin, which could be approximated by an extensional flow of the form

$$\mathbf{u} = (u, v) = \alpha(Wi)(x, -y)$$

While this remains true in the simulations with $\nu > 0$, we observe something slightly different here. In Fig. 1(a) we show the first component of the velocity along the axis of extension, $u(x,0)$, after reaching steady state for simulations with $Wi = 5$, 10, 15, 20, and

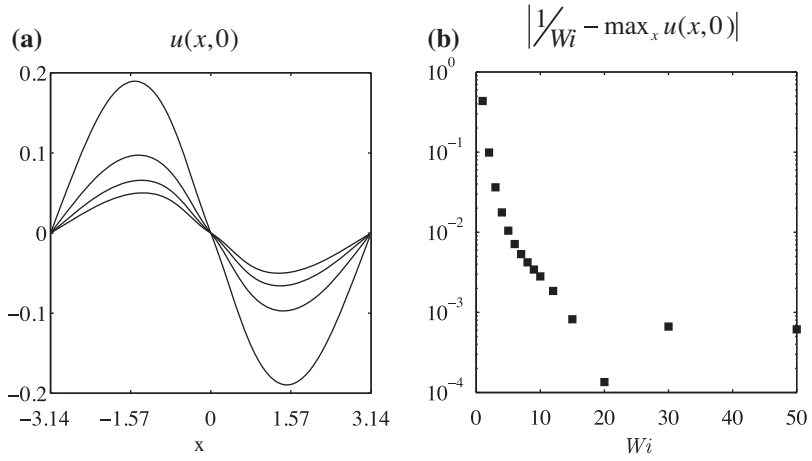

Fig. 1. (a) Velocity along axis of extension, u(x, 0), at steady state for $Wi = 5$, 10, 15, and 20, $\nu = .01$. Amplitudes are decreasing in Wi. (b) Absolute error in approximation of the amplitude of u in the direction of extension: $|1/Wi - \max_x u(x,0)|$.

$v = .01$ (the amplitudes are decreasing with increasing Wi). Solutions to Eq. (1) with no polymer stress ($\mathbf{S} = \mathbf{0}$) give $u(x,0) = \sin x$ and we see that the polymer stress appears to modify the flow along the axis of extension by changing the amplitude of the sine function $u(x,0) \approx \alpha(Wi)\sin x$. There do appear to be corrections to the sine function (most noticeably near $x = 0$ for higher Wi) however, the primary behavior is a change in amplitude of the $\mathbf{S} = \mathbf{0}$ flow. We take $\alpha(W\ i) = \max_x u(x,0)$. Fig. 1(b) shows the result of comparing the simulation result $\alpha(Wi) = \max_x u(x,0)$ with $1/Wi$ for a wide range of Weissenberg number. For the range of Wi we are most interested in, $5 < Wi < 30$, the error in this approximation is $\mathcal{O}(10^{-3})$, therefore it seems reasonable to assume a local (near $(x,y) = (0,0)$) extensional flow of the form

$$\mathbf{u} = \frac{1}{Wi}(x, -y). \tag{6}$$

In Fig. 2(a) a plot of max tr $\mathbf{S}$ for $Wi = 5$, 10, 15, and 20 as a function of t/Wi demonstrates the first qualitative difference between the results of simulations of the system for $v = 0$ (from [16]) and for $v > 0$. We see that when $v > 0$, the maximum value of the stress approaches a steady state for all Wi (our simulations include $0 < Wi \leqslant 50$). In [16] with $v = 0$ and Wi sufficiently large, the stress was shown to grow exponentially at extensional stagnation points, while here there is an initial period of growth followed by decay to a finite steady value. We investigate this value (which in Fig. 2(a) appears to grow linearly in Wi) further in Section 3. Fig. 2(b–d) displays contour plots of vorticity, tr $\mathbf{S}$, and S_{12} for $Wi = 10$ at steady state. The origin is an extensional point in the flow and in its neighborhood we see that tr $\mathbf{S}$ concentrates in thin islands (birefringent strands) along the direction of extension. The additional vortices seen in Fig. 2(b) were also seen in the Oldroyd-B model with no diffusion [16].

Now we discuss the consequences of assuming a steady velocity field of the form given in Eq. (6). When this steady flow is used with the Oldroyd-B constitutive model from Eqs. (2) and (4) the evolution equation for the conformation tensor decouples and is *independent of Wi*. In this case the steady-state equations to solve become

$$x\partial_x S_{11} - y\partial_y S_{11} - S_{11} = 1 + v\Delta S_{11}, \tag{7}$$
$$x\partial_x S_{12} - y\partial_y S_{12} + S_{12} = v\Delta S_{12}, \tag{8}$$
$$x\partial_x S_{22} - y\partial_y S_{22} + 3S_{22} = 1 + v\Delta S_{22}. \tag{9}$$

There is an exact solution for the stress tensor of the form:

$$S_{11} = -1 + Ae^{-\frac{y^2}{2v}}, \tag{10}$$
$$S_{12} = 0, \tag{11}$$
$$S_{22} = \frac{1}{3}. \tag{12}$$

This solution is chosen to match the behavior seen in the simulations, namely compression along the $y-$axis. We refer to the solution for S_{11} given in Eq. (12) as the approximate (Gaussian) solution and call it $\gamma(y)$ for convenience. Hence

$$\gamma(y) = -1 + Ae^{-\frac{y^2}{2v}}$$

For $v > 0$ γ is bounded and smooth, and in the limit $v \to 0$ γ approaches the delta function which matches the local solution in [16]. Next we examine the simulations and compare them to the Gaussian solution γ.

3. Numerical results for Oldroyd-B

Fig. 3 shows results of the simulation of $S_{11}(0,y)$ for $v = .01$, ranging in Weissenberg number, $1 \leqslant Wi \leqslant 20$, at $t = 10 \cdot Wi$, by which time solutions have reached steady state. We observe that max $S_{11}(0,y)$ occurs at $y = 0$ (and periodically due to the boundary conditions). These solutions appear to be nearly Gaussian with an inner-scale independent of Wi. Futhermore, max$S_{11}(0,y)$ appears to

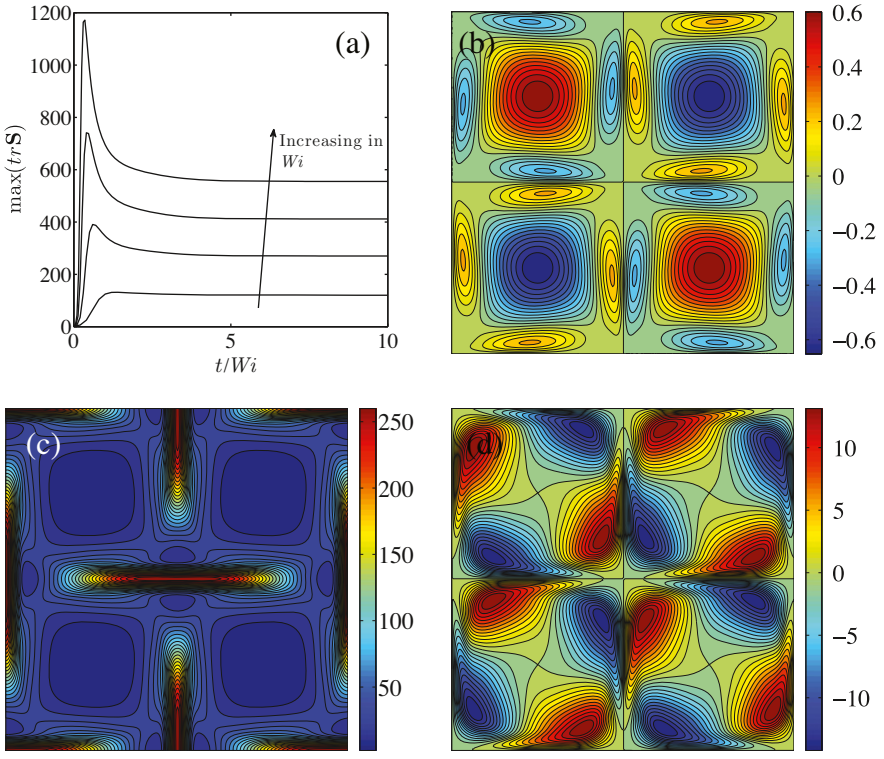

Fig. 2. (a) max tr $\mathbf{S}$ for $Wi = 5$, 10, 15, and 20 ($v = .01$) plotted versus t/Wi, by $t = 10 \cdot Wi$ solutions have reached steady state. (b–d) contour plots of vorticity, tr $\mathbf{S}$, and S_{12} for $Wi = 10$ at steady state.

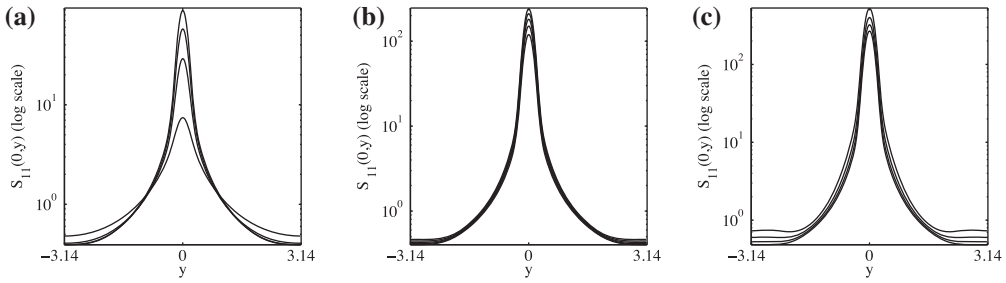

Fig. 3. Plot of $S_{11}(0,y)$ (log scale) with $v = .01$ for (a) $Wi = 1, 2, 3, 4$ (increasing in Wi); (b) $Wi = 5, 6, 7, 8, 9$; (c) $Wi = 10, 12, 15, 20$.

grow linearly in the Weissenberg number. We analyze both of these conjectures now.

We would like to compare the steady state profile of $S_{11}(0,y)$ with the Gaussian solution $\gamma(y) = -1 + Ae^{-\frac{y^2}{2v}}$. We compare the full width at half maximum for γ (in this case this value is $2\sqrt{2\ln 2v}$) with the simulation. The relative error in this comparison is shown in Fig. 4(a) varying both v and Wi. The error decreases as $v \to 0$ and for all v the error is smallest (around 15–20%) for moderate Weissenberg $5 \leqslant Wi \leqslant 10$.

Next we look at the conjecture that $S_{11}(0,0)$ grows linearly in Wi. Fitting $\log(Wi)$ with $\log(S_{11}(0,0))$ for each $v = .003, .005, .01, .02, .05$ yields exponents of the equation $S_{11}(0,0) = CWi^q$ to be $q = 1.074, 1.02, 0.99, 1.04$, and 1.12 indicating that as v gets sufficiently small a linear fit with Wi is quite reasonable. Fig. 4(b) shows the values of $S_{11}(0,0)$ at steady state for $Wi = 5 - 10, 12, 15, 20$ for $v = .005, .01, .02$, the dotted lines are linear fits to the data for $Wi = 5 \ldots .20$.

To further probe the amplitude for the approximate solution γ, we observe that the integral $I_S = \int_{-\pi}^{\pi} S_{11}(0,y)dy$ shows only slight dependence on v. Fitting $\log(I_S)$ with $\log(v)$ for $Wi = 5 \ldots 20$ yields exponents of the equation $I_S = Cv^q$ to be $.070 \leqslant q \leqslant .092$. Fig. 4(c) shows I_S as a function of v on a log scale for $Wi = 5 - 10$ (increasing in Wi). In order for γ to be independent of v we must have γ scale with $v^{-1/2}$. Fig. 4(d) shows the relative error in the approximation of $S_{11}(0,0)$:

$$\left|\frac{S_{11}(0,0) - CWiv^{-1/2}}{S_{11}(0,0)}\right|,$$

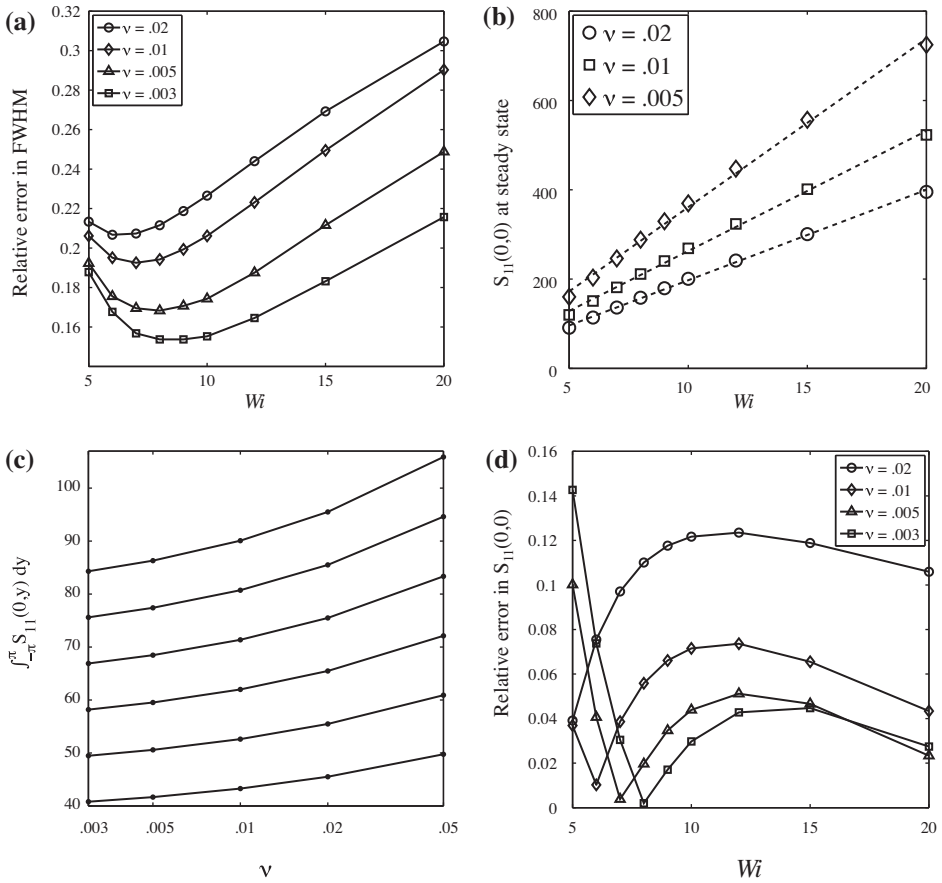

Fig. 4. (a) Relative error in the full-width at half maximum when comparing the Gaussian solution γ to simulated results. (b) Plot of $S_{11}(0,0)$ at steady state varying in Wi and v, dotted lines are linearly fit to the data. (c) Dependence of $\int_{-\pi}^{\pi} S_{11}(0,y)dy$ on v (log scale) for $Wi = 5 - 10$, increasing in Wi. (d) Relative error in the maximum polymer extension comparing the simulation $S_{11}(0,0)$ with the approximation of $\gamma(0) = -1 + CW\,iv^{-1/2}$.

where C is a constant, independent of Wi,v. Again we notice that this approximation improves as $v \to 0$ and the error is less than 5% for $v \leqslant .005$ and $5 \leqslant Wi \leqslant 10$.

These numerical tests combined with the local analysis gives us confidence that

$$S_{11}(0, y) \approx -1 + CWiv^{-1/2}e^{-y^2/2v}$$

is a reasonable approximation for the first component of the polymer stress near extensional points in the flow. This gives us the behavior of the stress as $v \to 0$ and indicates that adding polymer stress diffusion will yield a smooth and bounded polymer stress for all $v > 0$.

Finally we make some comments regarding the dependence of the steady solutions on β. Fig. 5(a) shows the velocity $u(x,0)$ for $\beta \cdot Wi = .5, 1, .25$ which we refer to as β_0, $2\beta_0$, $.5\beta_0$ (here we fix $Wi = 10$, $v = .01$). Changing β does not appear to change the velocity significantly and in fact the maximum difference between $\mathbf{u}_{\beta_0}$ and $\mathbf{u}_{2\beta_0}$ or $\mathbf{u}_{.5\beta_0}$ is .034. Fig. 5(b) shows the first component of the conformation tensor (rescaled for comparison) for $\beta \cdot Wi = .5, 1, .25$. It appears that when $\beta \cdot Wi$ is doubled (resp. halved) the conformation tensor is roughly halved (resp. doubled) to compensate. This is also consistent with the fact that the advection equation for the conformation tensor (Eq. (4)) is nearly homogeneous in $\mathbf{S}$ and the Stokes equation (Eq. (1)) is linear in $\mathbf{S}$. For the stress we have that the relative maximum difference between $\mathbf{S}_{\beta_0}$ and $2\mathbf{S}_{2\beta_0}$ or $.5\mathbf{S}_{.5\beta_0}$ is 10%. Although there is not a significant change in the flow upon changing β, as $\beta \to 0$ the polymer stress is increasing as well making numerical simulations more difficult as the stress and stress gradients grow. If we let $\beta \cdot Wi = \xi$ we can modify our scaling of max tr $\mathbf{S}$ to include ξ as

$$\max\ \text{tr}\ \mathbf{S} \approx C/2Wiv^{-1/2}\xi^{-1}$$

4. Finite extension

We turn now to the FENE-P model and investigate what can be learned from our local model when finite extensibility is enforced. The FENE-P model differs from the Oldroyd-B model by employing the extra stress tensor given in Eq. (3). This consists of substituting

$$\mathbf{S}^{\text{fp}} = \frac{\mathbf{S}}{1 - \frac{\text{tr}\mathbf{S}}{b}} \tag{13}$$

for $\mathbf{S}$ in Eq. (2). In FENE-P $\mathbf{S}^{\text{fp}}$ will diverge as the maximum of the trace of the conformation tensor approaches the extension parameter b. This penalization keeps tr $\mathbf{S}$ bounded away from b in simulations. In [16] it was numerically demonstrated that without another diffusion mechanism this penalization is not sufficient to keep the stress smooth. Large stress gradients and corners form in the stress for sufficiently large Wi. Therefore there is still a need for a smoothing mechanism as is gained by adding the diffusion term $v > 0$.

The effect of diffusion and finite extension are two distinct modifications to the model which arise from different microscopic origins and have different effects on the flow in general. For example; the FENE model results in shear-rate-dependence in the normal stresses at high Wi, whereas the numerical diffusivity of the Oldroyd-B model does not affect the quadratic scaling with Wi in homogeneous flows. However in many simulations of viscoelastic flows both a FENE-P cut-off and numerical diffusion are employed and we believe it is worth some investigation to see which effect dominates for various model parameters.

Fig. 6(a) (and zoom in (b)) shows $\mathbf{S}^{\text{fp}}_{11}(0, y)$ for $Wi = 10$ and $v = .005$ for $b = 25, 49, 225, 625$. We see that $\mathbf{S}^{\text{fp}}_{11}(0, 0)$ appears to be converging to a finite value (as $b \to \infty$) and increasing b further confirms this. As $b \to \infty$ the FENE-P model converges to the Oldroyd-B model so it is reasonable to assume that the value $\mathbf{S}^{\text{fp}}_{11}(0, 0)$ will approach is the value one would obtain from the Oldroyd-B simulation. With $Wi = 10$,$v = .005$, Oldroyd-B yields $\mathbf{S}^{\text{ob}}_{11}(0, 0) = 370$ at steady state, which is quite close to the value seen here for $b = 625$ where $\mathbf{S}^{\text{fp}}_{11}(0, 0) = 392$.

We can couple our prediction of max tr $\mathbf{S}^{\text{ob}} = C\ Wiv^{-1/2}$ coming from the local analytic model with the fact that for b sufficiently large $\mathbf{S}^{\text{fp}} \to \mathbf{S}^{\text{ob}}$ to predict the percent of extension (or fraction of b) the FENE-P simulation will yield at extensional points in the flow. We suppose that the maximum of the conformation tensor extends to some fraction of the maximum extension parameter, i.e. max tr $\mathbf{S} = rb$ for some $0 < r < 1$ and using monotonicity and Eq. (13) we have that

$$\max \text{tr}\ \mathbf{S}^{\text{fp}} = \frac{r}{1-r}b. \tag{14}$$

Now as $b \to \infty$ the FENE-P model approaches the Oldroyd-B model, so for sufficiently large b, it is reasonable to assume that the effect of diffusion on max tr $\mathbf{S}^{\text{fp}}$ will dominate the effect of finite extensibility. In that case we assume that max tr $\mathbf{S}^{\text{fp}} \approx CWiv^{-1/2}$. Therefore we can predict the percent extension r in Eq. (14) in terms of v, Wi, b as

$$r = \frac{CWiv^{-1/2}b^{-1}}{1 + CWiv^{-1/2}b^{-1}}$$

The quantity $CWiv^{-1/2}b^{-1}$ can be used to measure which effect (diffusion or finite extension) is dominating the problem. If $CWiv^{-1/2}b^{-1} \ll 1$ diffusion will be responsible for setting the scale of max tr $\mathbf{S}^{\text{fp}}$ and if $C\ Wiv^{-1/2}b^{-1} \gg 1$ polymers will extend near to the enforced FENE-P cut-off. These limits are consistent with our

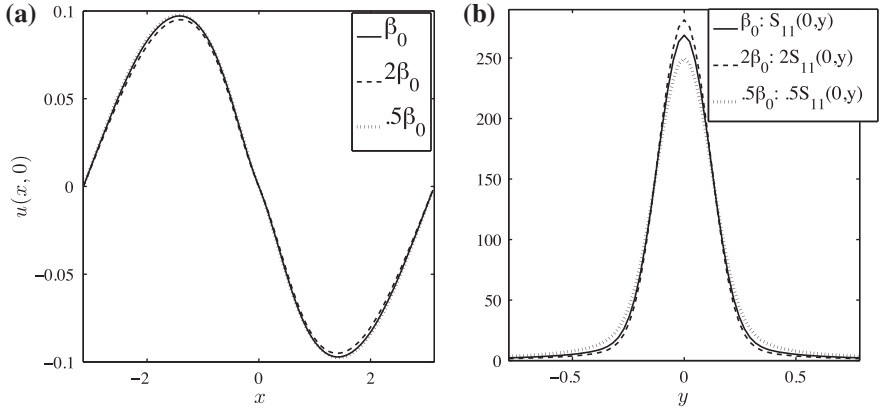

Fig. 5. (a) $u(x,0)$ for $\beta \cdot Wi = .5, 1, .25$ with $Wi = 10$,$v = .01$ (b) First component of conformation tensor along direction of compression while varying β.

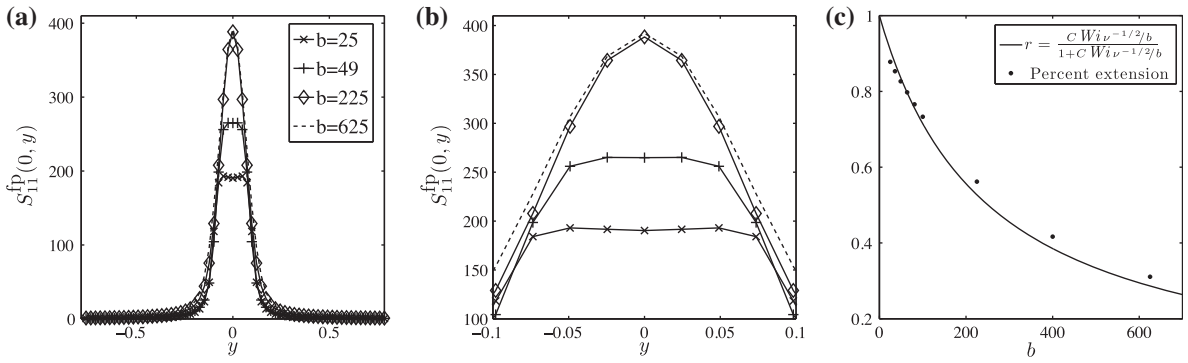

Fig. 6. (a) Plot of $\mathbf{S}_{11}^{fp}(0, y)$ for $Wi = 10$, $\nu = .005$ and $b = 25, 49, 225, 625$. (b) Zoom of (a) with same figure annotations. (c) Plot of comparison of the theoretical prediction with the simulated values of the percent of extension for $Wi = 10$, $\nu = .01$.

understanding of the problem and the intermediate to high range of this parameter is the most interesting. In Fig. 6(c) we plot the theoretical prediction for this percent of extension in the case where $Wi = 10$, $\nu = .01$ as a function of the extension parameter b and compare this with the simulated values of max tr $\mathbf{S}^{fp}/b$. In these and other simulations the relative error in the prediction of r varies from <1% to 9% for Wi ranging from 10 to 20 and for $\nu = \mathcal{O}(10^{-2}, 10^{-3})$.

Fig. 7 shows results from simulations with higher Wi. Fig. 7(a and b) displays contour plots of tr $\mathbf{S}^{fp}$ and vorticity for $Wi = 50$, $b = 1024$, $\nu = .01$ while Fig. 7(c and d) shows the same plots for an order of magnitude smaller diffusion. For $\nu = .01$ and $Wi = 50$ the Oldroyd-B amplitude prediction would be $A = 1253$, and with $b = 1024$, we have a predicted extension percent of $r = 0.55$. In the simulations at steady state max tr $\mathbf{S} = 575 = 0.56 \cdot b$, a relative error in our prediction of 2%. We notice that in this simulation max tr $\mathbf{S}^{fp}$ no longer occurs at the origin but has shifted to $(\pm 5/8\pi, 0)$, though the reason for this is not clear. For $\nu = .001$ we have $A = 3963$ which gives $r = 0.79$. In the simulations at steady state max tr $\mathbf{S} = 837 = 0.81 \cdot b$, a relative error in our prediction of 3.5%.

Fig. 8 shows the vorticity for two FENE-P simulations with $Wi = 10$, $\nu = .001$ and $b = 4$ panel (a) and $b = 100$ panel (b). We observe that the additional vortices seen in simulations for Oldroyd-B for sufficiently large Wi (as in Fig. 2(b)) and those seen in panel (b) are suppressed in panel (a). We interpret this major qualitative difference in the solution to mean that b is too small and the polymers are not allowed to extend sufficiently to create enough

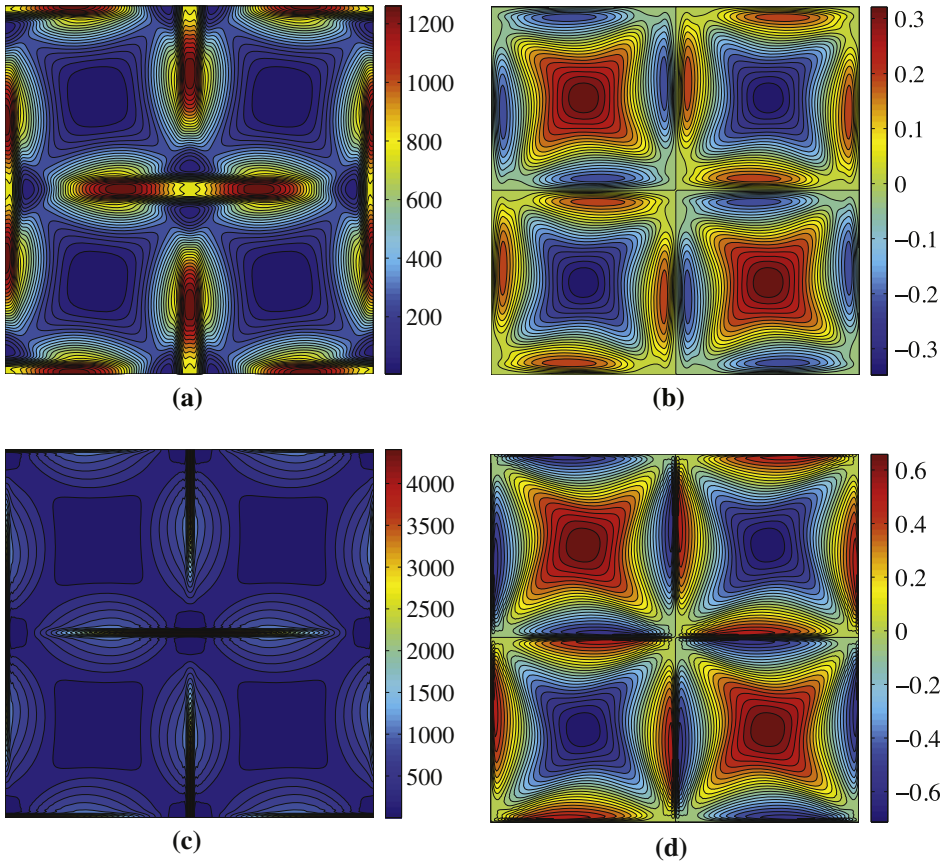

Fig. 7. (a and b) Contour plots of (a) tr $\mathbf{S}^{fp}$ and (b) vorticity for $Wi = 50$, $\nu = .01$, $b = 1024$ at steady state. (c and d) Contour plots of (a) tr $\mathbf{S}^{fp}$ and (b) vorticity for $Wi = 50$, $\nu = .001$, $b = 1024$ at steady state.

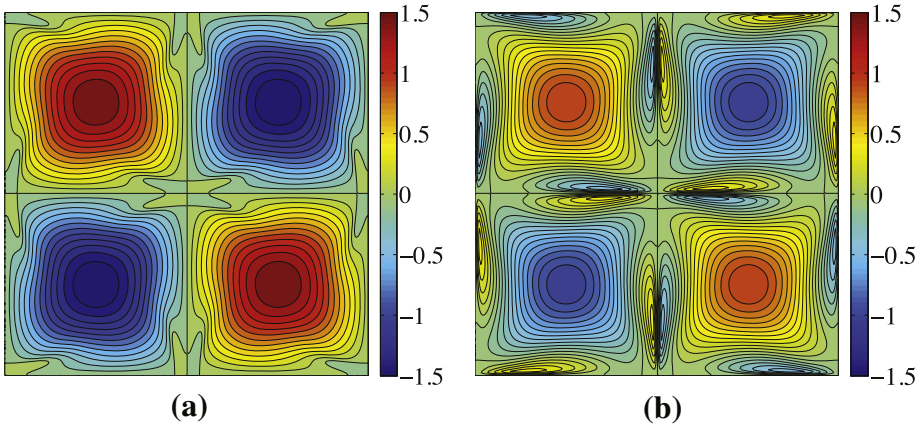

Fig. 8. Vorticity for FENE-P fluid with $Wi = 10$, $v = .001$ (a) $b = 4$ (b) $b = 100$.

extra stress along the outgoing streamlines of the extensional point. For fixed Wi,v one can choose b sufficiently small to be sure that the cut-off mechanism is coming from the FENE-P penalization, however if b is chosen too small than the response of the flow is altered significantly from what is seen in the Oldroyd-B model or the FENE-P model for larger b.

5. Conclusions

Based on numerical simulations we see that adding stress diffusion keeps the conformation tensor bounded and smooth. Furthermore we observe that at extensional points in the flow the velocity field is a local straining flow of the form $\mathbf{u} = \frac{1}{Wi}(x, -y)$. With this assumption there is an exact solution for the stress tensor which is Gaussian in y with the width scaling with the square root of the diffusion. This implies that for any amount of diffusion the conformation tensor is bounded and smooth, though numerical difficulties will still arise in resolving a solution with a physically realistic level of stress diffusion. The amplitude of the exact solution can be approximated giving a scaling for max tr $\mathbf{S} \sim W i v^{-1/2}$.

MHD flows driven by forcing such as (5) have been studied extensively and the "birefringent strands" seen in Figs. 2(c) and 7(a and c) are reminiscent of flux tube structures in magneto-convection. In particular the analytic solution given in Eq. (12) is analogous to the inner solution found in [28] for magnetic flux ropes. A formal comparison between the Oldroyd-B equations in the high Wi limit to the MHD equations in the large magnetic Reynolds number limit was made in [29]. The author gratefully acknowledges one of the referees for pointing out this connection and plans to investigate it further.

When a FENE-P penalization term is added to enforce finite extension of polymers we are able to use the scaling of the maximum of the conformation tensor to predict for a given Weissenberg number, diffusion coefficient, and maximum extension, the fraction of the maximum that the polymers will extend. This, in turn, gives a prediction of whether the scale of the maximum extension is determined by diffusion or if the polymers are allowed to extend to a large percentage of the upper bound on extension. The key parameter is

$$Wiv^{-1/2}b^{-1};$$

if this value is small the simulation is diffusion dominated. We see that keeping b small (relative to the diffusion) will ensure that polymers will extend to a large percent of the upper bound, however artificially keeping b small in order to enforce the FENE-P cut-off does change the flow dynamics.

Both diffusion and FENE-P enforce a cut-off on the maximum of the trace of the conformation tensor, but the physical effects are significantly different. Diffusion acts by moving molecules away from the extensional point and thereby reducing the overall effect of the stretching from the flow. The FENE-P model simply cuts off the trace of the conformation tensor and does not add any smoothness. Without going to higher closures of the FENE model or the full FENE model it appears that artificially large stress diffusion is still necessary to numerically resolve the large stresses and stress gradients that arise in the Oldroyd-B and FENE-P models.

Acknowledgements

The author thank Joseph Biello and Michael Shelley for many stimulating conversations related to this work.

References

[1] C.D. Dimitropoulos, R. Sureshkumar, A.N. Beris, Direct numerical simulation of viscoelastic turbulent channel flow exhibiting drag reduction: effect of the variation of rheological parameters, J. Non-Newtonian Fluid Mech. 79 (1998) 433–468.
[2] K.D. Housiadas, A.N. Beris, Polymer-induced drag reduction: effects of variations in elasticity and inertia in turbulent viscoelastic channel flow, Phys. Fluids 15 (2003) 2369–2384.
[3] P.K. Ptasinski, B.J. Boersma, F.T.M. Nieuwstadt, M.A. Hulsen, B.H.A.A. van den Brule, J.C.R. Hunt, Turbulent channel flow near maximum drag reduction: simulations, experiments and mechanisms, J. Fluid Mech. 490 (2003) 251–291.
[4] K.D. Housiadas, A.N. Beris, R.A. Handler, Viscoelastic effects on higher order statistics and on coherent structures in turbulent channel flow, Phys. Fluids 17 (2005). 035106.
[5] C.F. Li, R. Sureshkumar, B. Khomami, Influence of rheological parameters on polymer induced turbulent drag reduction, J. Non-Newtonian Fluid Mech. 140 (2006) 23–40.
[6] K. Kim, C.F. Li, R. Sureshkumar, S. Balachandar, R.J. Adrian, Effects of polymer stresses on eddy structures in drag-reduced turbulent channel flow, J. Fluid Mech. 584 (2007) 281–299.
[7] L. Xi, M. Graham, Active and hibernating turbulence in minimal channel flow of newtonian and polymeric fluids, Phys. Rev. Lett. 104 (2010). 218301.
[8] D. Richter, G. laccarino, E. Shaqfeh, Simulations of three dimensional viscoelastic flows past a circular cylinder at moderate reynolds numbers, J. Fluid Mech. 651 (2010) 415–442.
[9] A. Groisman, V. Steinberg, Elastic turbulence in a polymer solution flow, Nature 405 (2000) 53–55.
[10] A. Groisman, V. Steinberg, Efficient mixing at low Reynolds numbers using polymer additives, Nature 410 (2001) 905–908.
[11] A. Groisman, V. Steinberg, Elastic turbulence in curvilinear flows of polymer solutions, New J. Phys. 4 (2004). 74437–7.
[12] B. Thomases, M. Shelley, Transition to mixing and oscillations in a Stokesian viscoelastic flow, Phys. Rev. Lett. 103 (2009) 094501.
[13] B. Thomases, M. Shelley, J.-L. Thiffeault, A Stokesian viscoelastic flow: transition to oscillations and mixing, Phys. D (2011), doi:10.1016/j.physd.2011.06.011.
[14] J.M. Rallison, E.J. Hinch, Do we understand the physics in the constitutive equation?, J Non-Newtonian Fluid Mech. 29 (1988) 37–55.

[15] M. Renardy, A comment on smoothness of viscoelastic stresses, J. Non-Newtonian Fluid Mech. 138 (2006) 204–205.
[16] B. Thomases, M. Shelley, Emergence of singular structures in Oldroyd-B fluids, Phys. Fluids 19 (2007) 103103.
[17] R.B. Bird, O. Hassager, R.C. Armstrong, C.F. Curtiss, Dynamics of Polymeric Liquids, Kinetic Theory, vol. 2, John Wiley and Sons, 1980.
[18] R.G. Larson, The Structure and Rheology of Complex Fluids, Oxford University Press, 1998.
[19] R. Sureshkumar, Antony N. Beris, Effect of artificial stress diffusivity on the stability of numerical calculations and the flow dynamics of time-dependent viscoelastic flows, J. Non-Newtonian Fluid Mech. 60 (1) (1995) 53–80.
[20] P.E. Arratia, C.C. Thomas, J. Diorio, J.P. Gollub, Elastic instabilities of polymer solutions in cross-channel flow, Phys. Rev. Lett. 96 (2006) 144502.
[21] A.W. El-Kareh, L.G. Leal, Existence of solutions for all Deborah numbers for a non-Newtonian model modified to include diffusion, J. Non-Newtonian Fluid Mech. 33 (1989) 257.
[22] J.T. Beale, T. Kato, A. Majda, Remarks on the breakdown of smooth solutions for the 3-d Euler equations, Comm. Math. Phys. 94 (1984) 61–66.
[23] J.Y. Chemin, N. Masmoudi, About lifespan of regular solutions of equations related to viscoelastic fluids, SIAM J. Math. Anal. 33 (2001) 84–112.
[24] R. Kupferman, C. Mangoubi, E. Titi, A Beale-Kato-Majda breakdown criterion for an Oldroyd-B fluid in the creeping flow regime, Commun. Math. Sci. 6 (2008) 235–256.
[25] N. Balci, B. Thomases, M. Renardy, C. Doering, Symmetric factorization of the conformation tensor in viscoelastic fluid models, J. Non-Newtonian Fluid Mech. 166 (2011) 546–553.
[26] Roger Peyret, Spectral Methods for Incompressible Viscous Flow, Springer, New York, 2002.
[27] T.Y. Hou, R. Li, Computing nearly singular solutions using pseudo-spectral methods, J. Comput. Phys. 226 (2007) 379–397.
[28] D.J. Galloway, M.R.E. Proctor, N.O. Weiss, Magnetic flux ropes and convection, J. Fluid Mech. 87 (1978) 243–261.
[29] G.I. Ogilvie, M.R.E. Proctor, On the relation between viscoelastic and magnetohydrodynamic flows and their instabilities, J. Fluid Mech. 476 (2003).